Applied Catalysis B: Environmental 246 (2019) 232–241

Contents lists available at ScienceDirect

Applied Catalysis B: Environmental

journal homepage: www.elsevier.com/locate/apcatb

Synthesis of mixed alcohols with enhanced C3+ alcohol production by CO hydrogenation over potassium promoted molybdenum sulfide

Feng Zeng[a,1], Xiaoying Xi[b,1], Huatang Cao[c], Yutao Pei[c], Hero Jan Heeres[b,*], Regina Palkovits[a,*]

[a] Chair of Heterogeneous Catalysis and Chemical Technology, ITMC, RWTH Aachen University, Worringerweg 2, 52074, Aachen, Germany
[b] Green Chemical Reaction Engineering, Engineering and Technology Institute Groningen, University of Groningen, Nijenborgh 4, 9747 AG, Groningen, the Netherlands
[c] Department of Advanced Production Engineering, Engineering and Technology Institute Groningen, Faculty of Science and Engineering, University of Groningen, Nijenborgh 4, 9747AG, the Netherlands

ARTICLE INFO

Keywords:
Syngas
Mixed alcohols
Fuel additives
Molybdenum disulfide
Carbon chain growth

ABSTRACT

Alcohol mixtures with high C3+ alcohols content can enhance the performance of alcohol mixtures as a blend component in gasoline. Sulfur-resistant potassium promoted molybdenum sulfide (K-MoS_2) catalysts enabled synthesizing mixed alcohols through CO hydrogenation. However, the liquid oxygenate selectivity and yield of K-MoS_2 catalysts are usually low, and the alcohols follow the Anderson-Schulz-Flory (ASF) distribution, which means methanol and ethanol present the main liquid oxygenates. To achieve high liquid oxygenate selectivity and yield enhancing C3+ alcohol production, we designed multilayer K-MoS_2 catalysts possessing a well-contacted MoS_2 and $KMoS_2$ phase, respectively. The reduced rim site exposure and the well-contacted MoS_2-$KMoS_2$ dual site induced by the multilayer structure enhance the chain growth through CH_x β-addition and CO insertion. Accordingly, the observed higher alcohol formation deviates from the ASF distribution. By tailoring the K/Mo ratio, catalysts with varying composition of MoS_2 and $KMoS_2$ phases were obtained for suppressing the formation of hydrocarbons and CO_2 effectively. An optimized production of liquid oxygenates with enhanced C3+ alcohol production under appropriate reaction temperature became possible. The optimized catalysts have liquid oxygenate selectivity and yield of 29.1–32.7% and 7.9–10.6%, respectively, yet with good stability. C3+ alcohols take up more than 46% (carbon atom fraction) in the liquid oxygenate. The C3+ alcohol yield reaches 3.6–5.1%.

1. Introduction

Since world's crude oil reserves are quickly consumed, alternatives for gasoline like alcohols, natural gas, and hydrogen are indispensable for a sustainable society [1–6]. Alcohols including methanol and ethanol have been intensively studied and used as gasoline blend components [6–8]. However, methanol and ethanol hold low energy density, high vapor pressure, and high affinity to water leaving room for further improvement [9,10]. Compared with methanol and ethanol, C3+ alcohols generally possess higher energy density and lower vapor pressure, and C3+ alcohols like butanol exhibit a lower affinity to water. The octane number of C3+ alcohols is also comparable to gasoline [9,10]. Thus alcohol mixtures with high C3+ alcohol content may help to improve the performance as a gasoline blend component.

Alcohols can be synthesized by the catalytic conversion of syngas, the fermentation of sugars, and the hydration of petroleum-derived alkenes [11–13]. Since syngas could be produced through various routes and feedstock such as biomass gasification, natural gas reforming, and CO_2 reduction, the direct catalytic conversion of syngas provides high sustainability and is very appealing for the direct mixed alcohols production [14–17]. The catalytic conversion of syngas to mixed alcohols comprehends alcohol formation as the major reaction, together with hydrocarbon formation and the water-gas-shift reaction as main side reactions [18].

Alcohol formation: $nCO + 2nH_2 \leftrightharpoons C_nH_{2n+1}OH + (n-1)H_2O$ (1)

Hydrocarbon formation: $nCO + (2n+1)H_2 \leftrightharpoons C_nH_{2n+2} + nH_2O$ (2)

Water-gas-shift: $CO + H_2O \leftrightharpoons CO_2 + H_2$ (3)

The most intensively studied catalysts for mixed alcohols' synthesis from syngas include rhodium-based catalysts, molybdenum-based systems, modified Fischer-Tropsch synthesis catalysts, and modified

* Corresponding authors.
E-mail addresses: h.j.heeres@rug.nl (H.J. Heeres), palkovits@itmc.rwth-aachen.de (R. Palkovits).
[1] These authors have contributed equally to this work.

https://doi.org/10.1016/j.apcatb.2019.01.063
Received 23 October 2018; Received in revised form 16 January 2019; Accepted 19 January 2019
Available online 23 January 2019

methanol synthesis catalysts [13]. Among them, molybdenum sulfide-based materials exhibit promising performance and significant sulfur-resistance avoiding the costly deep desulfurization of syngas [19,20]. Even though sole MoS_2 produces mainly hydrocarbons, alkali metal promoted molybdenum disulfide enables increasing selectivity for alcohols [21]. Alkali metals, for example potassium (K), are supposed to form potassium-containing species like $KMoS_2$ and K_2MoS_2, which are relevant for the formation of alcohols [13,22]. A dual site model is proposed for the conversion of syngas to mixed alcohols over transition metal promoted potassium-doped molybdenum sulfide (K-MoS_2) catalysts. CO dissociative adsorption, H_2 dissociative adsorption, and CH_x formation take place on the transition metal sulfide phase (MS_x, M = Fe, Co, or Ni), and methane is formed by direct hydrogenation of CH_x species. Non-dissociative CO adsorption, chain growth, and alcohol formation take place on the potassium promoted metal sulfide phase (K-MMoS) [18,23]. The carbon chain growth comprises CO insertion and C1 intermediate addition. Linear primary alcohols are formed through CO insertion, while branched alcohols form via C1 intermediate addition [18,24].

Even though alkali metal promotion shifts the product selectivity from hydrocarbons to alcohols, the selectivity and yield of alcohols are usually low and hinder the successful commercialization of mixed alcohol synthesis from syngas [25]. Besides, the alcohol product possesses a selectivity order of methanol > ethanol > propanol obeying Anderson-Schulz-Flory (ASF) distribution [19,26]. Accordingly, C3+ alcohols take up less than 30% (carbon atom fraction) of the alcohols [20,24,26–28]. Nickle, cobalt, and lanthanum are reported as promoters to enhance the chain growth over K-MoS_2 catalysts allowing to deviate from the ASF distribution [24,26–28]. Therewith, the C3+ alcohol content reaches about 50% (carbon atom fraction) of the alcohol product. Except for promoters, the structure of MoS_2 is also of significant importance to enhance chain growth and to boost C3+ alcohols production. Dorokhov et al. propose that the active centers for mixed alcohols synthesis are located on the edges of two adjacent K-MoS_2 layers [29]. The adsorbed methyl fragment can participate in chain growth with other adsorbed species on the adjacent layers. Therefore, edge sites of multilayer K-MoS_2 are more favorable for chain growth with methyl fragment participation than rim sites or fewer stacked K-MoS_2, which hold less adjacent layers. The C3+ alcohol selectivity can also be enhanced by tailoring the MoS_2 double layer structure [30]. Even though C3+ alcohol content reaches about 50% (carbon atom fraction) in the alcohols product, the overall yield of C3+ alcohols accounts for less than 2%, clearly leaving space for further improvement [30].

Herein we report a method to prepare multilayer K-MoS_2 catalysts for converting syngas to mixed alcohols with high selectivity and yield together with an enhanced C3+ alcohol production. Thermal treatment of a mixture of amorphous molybdenum sulfide precursor with K_2CO_3 leads to the formation of a multilayer K-MoS_2 structure with well-contacted MoS_2 phase and $KMoS_2$ phase, which are the bifunctional active centers for mixed alcohols synthesis. The reduced rim site exposure and well-contacted MoS_2-$KMoS_2$ dual site due to the multilayer structure boost C3+ alcohol formation and allow deviating from ASF distribution of the alcohols through enhanced CO insertion and CH_x β-addition. The potassium loading is optimized to obtain K-MoS_2 with varying content of MoS_2 and $KMoS_2$ to inhibit hydrocarbons and CO_2 formation, and enhance alcohols formation with enhanced C3+ alcohol production under appropriate reaction temperature to reach high liquid oxygenate selectivity and yield. The optimized catalysts enable high liquid oxygenate selectivity and yield, together with an enhanced C3+ alcohol yield reaching 29.1–32.7%, 7.9–10.6%, and 3.6–5.1%, respectively. C3+ alcohols take up more than 46% (carbon atom fraction) in the liquid oxygenate. We therewith contribute a new method to deviate from the ASF distribution of alcohols with high C3+ alcohol yield over MoS_2 based catalyst by designing the structure of K-MoS_2 catalyst without nickel, cobalt, or lanthanum promoter.

2. Experimental

2.1. Catalyst preparation

The amorphous molybdenum sulfide precursor was prepared by the method reported in [31]. Generally, molybdenum sulfide was precipitated by mixing 5 mL 15.0% $(NH_4)_6Mo_7O_{24}{\cdot}4H_2O$ (Fluka) solution with 5 mL 34.6% $Na_2S{\cdot}9H_2O$ (Sigma-Aldrich) solution in 88 mL 4.0% hydrochloric acid (Fluka) solution. The obtained dark brown slurry was kept under 80 °C with stirring and reflux. 0.7 g $HONH_2{\cdot}HCl$ (Sigma-Aldrich) was added to the mixture after half an hour. The slurry was filtered and washed with deionized water after one more hour, followed by drying in atmospheric condition. Thereby the amorphous molybdenum sulfide precursor was obtained with less than 0.08 wt% sodium impurity (inductively coupled plasma optical emission spectrometry). Potassium was incorporated into the catalyst by physical mixing of the amorphous molybdenum sulfide precursor with K_2CO_3 (Sigma-Aldrich) in a mortar with a pestle followed by treatment at 500 °C in hydrogen atmosphere for 3 h with a heating rate of 5 °C/min. The amount of K_2CO_3 was varied to adjust the K/Mo mole ratio from 0 to 0.52.

2.2. Catalyst characterization

N_2-physisorption was used to measure the surface area, the pore volume, the pore diameter, and the pore diameter distribution of the catalyst. The measurement was performed on an ASAP 2420 analyzer. The specific surface area was calculated with Brunauer–Emmett–Teller (BET) method. The pore volume was calculated using single point desorption data at $P/P_o = 0.97$. The pore diameter and pore diameter distribution were calculated with Barrett-Joyner-Halenda (BJH) method using the desorption branch. X-ray diffraction (XRD) analyses were performed on a D8 Advance Bruker diffractometer with a CuK_α 1 radiation ($\lambda = 1.5418$ Å). The XRD patterns were collected under 40 kV and 40 mA in the 2theta range of 5°-80°. Attenuated total reflection-Fourier transform infrared (ATR-FTIR) spectra were collected on a Bruker VERTEX 70 spectrometer equipped with an ATR geometry, in the wave number range of 400-4000 cm^{-1} with a resolution of 4 cm^{-1}. SPECTROBLUE ICP-OES (inductively coupled plasma optical emission spectrometry) was used to determine the potassium/molybdenum ratio. Electron probe microanalysis (EPMA) was carried out on a JEOL JXA-8530 F electron probe microanalyzer to study the distribution of potassium promoter. Raman spectroscopy was performed on a WITec Alpha 300R microscope with a 532 nm excitation laser. High resolution transmission electron microscopy (HRTEM) images were obtained with a JEOL 2010-FEG microscope operating at 200 kV. The X-ray photoelectron spectra (XPS) were obtained by a SSX-100 (Surface Science Instruments) photoelectron spectrometer using a monochromatic Al Kα X-ray source ($h\nu = 1486.6$ eV).

2.3. Catalytic reaction test

To evaluate the catalytic performance in the conversion of syngas to mixed alcohols, the catalysts were tested using a high-pressure fixed bed reactor (10 mm inner diameter) setup. The gas mixture with a H_2/CO/N_2 volume ratio of 47:47:6 was mixed and pressurized by a high-pressure compressor before entering the reactor. The flow rate of gas mixture was controlled by a high-pressure mass flow controller. The reactor was located in an oven to keep the reaction temperature. The exit stream from the reactor was cooled and separated by a double walled condenser at -5 °C. The gas products were analyzed by an online gas chromatograph (Compact GC, Interscience BV). The liquid products were collected during steady operation and were analyzed by an offline gas chromatograph (Finnigan TRACE GC Ultra, Thermo Scientific). Typically, the reactor was loaded with a layer of SiC (Sigma-Aldrich) at the bottom of the reactor, then a layer of the catalyst (0.40 g), and again

a layer of SiC on the top of the catalyst. The reactions were investigated under a gas hourly space velocity (GHSV) of 4500 mL g^{-1} h^{-1}, a reaction pressure of 8.7 MPa, and at three temperatures of 300, 340 and 380 °C, respectively. External and internal mass transfer were excluded according to the methods reported in references [32,33]. The CO conversion, the product selectivity and yield were calculated with the following formulas. All the data reported in this article hold a carbon balance of higher than 95%. Methanol and ethanol loss was estimated by the online gas chromatograph. The identification and quantification of methanol and ethanol in gas phase were performed by passing nitrogen through a gas-washing bottle, which is filled with methanol or ethanol, and through the gas chromatograph at fixed flow rate. The carbon selectivity of methanol and ethanol in gas phase was calculated by formula (5).

CO conversion, X_{CO}, was calculated by

$$X_{CO} = \frac{moles\ of\ CO_{influent} - moles\ of\ CO_{effluent}}{moles\ of\ CO_{influent}} \times 100\% \quad (4)$$

Carbon selectivity of product i, S_i, was calculated by

$$S_i = \frac{moles\ of\ product\ i \times number\ of\ carbons\ in\ product\ i}{moles\ of\ CO_{influent} - moles\ of\ CO_{exfluent}} \times 100\% \quad (5)$$

Yield of liquid oxygenate, Y, was calculated by

$$Y = X_{CO} \times S_{liquid\ oxygenate} \quad (6)$$

ASF distribution was calculated based on

$$\frac{S_n}{n} = \alpha^{n-1} \times (1 - \alpha) \quad (7)$$

S_n% is the selectivity of the alcohols with a carbon number of n, n is the carbon number, and α is the chain growth probability. $\ln(\alpha)$ is the slope obtained by plotting $ln(\frac{S_n}{n})$ against $(n - 1)$.

3. Results and discussion

3.1. Synthesis of potassium promoted MoS_2 catalysts

The catalysts were prepared by thermal treatment of a mixture of $MoS_{3.7}$ (ICP-OES) precursor with K_2CO_3, and a series of K-MoS_2 catalysts were obtained by varying the weight ratio of K_2CO_3/$MoS_{3.7}$. Table 1 summarizes the physical and chemical properties of the catalysts. The catalysts (M0, M1, M2, M3, M4, and M5) possess K/Mo mole ratios ranging from 0 to 0.52 (S/Mo mole ratio is shown in Table S1). With increasing K/Mo ratio, the BET specific surface area and the pore volume decrease, while all the catalysts possess similar pore diameters of about 230 Å and similar pore size distributions (Fig. S1). The decrease of the specific surface area and the pore volume may be ascribed to partial blockage of the pores by potassium with increasing K/Mo ratio.

Fig. 1 presents the XRD patterns of the as-precipitated catalyst precursor and the thermal treated catalysts. The as-precipitated catalyst

Table 1
Physical and chemical properties of the catalysts.

Catalyst	$R_{K/Mo}$ [a]	S_{BET} [b], $m^2\ g^{-1}$	V_{sgp} [c], $cm^3\ g^{-1}$	D_{BJH} [d], Å
M0	0	40	0.25	257
M1	0.08	32	0.20	192
M2	0.15	30	0.18	206
M3	0.22	24	0.14	196
M4	0.38	13	0.09	239
M5	0.52	12	0.09	275

[a] K/Mo mole ratio by ICP-OES.
[b] Specific surface area by BET method.
[c] Single point pore volume.
[d] Pore diameter by BJH method.

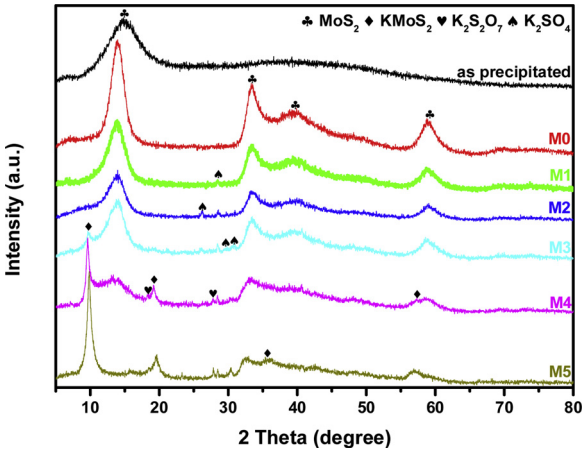

Fig. 1. XRD patterns of the as precipitated catalyst precursor and thermal treated catalysts with varying K/Mo ratio. K/Mo ratios of M0, M1, M2, M3, M4, and M5 are 0, 0.08, 0.15, 0.22, 0.38, and 0.52, respectively.

precursor, $MoS_{3.7}$, shows only one broadened 002 reflex of 2H-MoS_2 (JCPDS card No. 01-073-1508) at 2θ of about 14°, indicating an amorphous structure. After treatment at 500 °C in H_2 atmosphere, the obtained M0 possesses identical reflexes of crystalized 2H-MoS_2. The addition of potassium leads to the formation of potassium-containing species like $KMoS_2$ (JCPDS card No. 00-018-1064), K_2SO_4 (JCPDS card No. 01-070-1488) and $K_2S_2O_7$ (JCPDS card No. 00-001-0717). The $KMoS_2$ phase is essential for the formation of mixed alcohols; however, no corresponding reflexes occur for low K/Mo ratios (M1 and M2), maybe due to very small and therewith X-ray amorphous $KMoS_2$ crystallites. The characteristic reflex of $KMoS_2$ at 2θ of 10° appears for a K/Mo ratio of 0.22 (M3). The down shift of the 002 reflex from 14° to 10° 2θ indicates an expanded interlayer space and the insertion of potassium into the interlayer space of MoS_2, while the in-plane lattice parameter of pristine MoS_2 is maintained [34–36]. With increasing K/Mo ratio, the formation of $KMoS_2$ increases, while the amount of MoS_2 phase decreases. Thus, a mixture with adjacent MoS_2 and $KMoS_2$ layer structure could be obtained. Other potassium-containing species like K_2SO_4 and $K_2S_2O_7$, which may cover the active MoS_2 and $KMoS_2$ sites are found with increasing K/Mo ratio. The existence of K_2SO_4 and $K_2S_2O_7$ is further confirmed by ATR-FTIR spectra (Fig. S2). Even though the unpromoted catalyst (M0) exhibits no bands in ATR-FTIR spectra, because MoS_2 is black, the promoted catalysts (M1, M2, M3, M4, and M5) possess bands of K_2SO_4 and $K_2S_2O_7$. With increasing K/Mo ratio, the bands get stronger, indicating more K_2SO_4 and $K_2S_2O_7$. The formation MoO_3 was also detected by ATR-FTIR with high K/Mo ratio (M4 and M5).

Fig. 2 shows SEM images and elemental mappings of molybdenum, sulfur, and potassium for potassium promoted catalysts obtained by EPMA. With low K/Mo ratio (M1 and M2), potassium distributes homogeneously. Obvious aggregation of potassium is observed with a K/Mo ratio of 0.22 (M3). With higher K/Mo ratio (M4 and M5), more intensive aggregation of potassium is found. The excessive addition of potassium leads to the formation of inactive K_2SO_4 and $K_2S_2O_7$ as inferred by XRD and ATR-FTIR results, and the aggregation of inactive potassium-containing species, which may block the catalyst pore structure and cover the active sites.

Fig. 3 shows TEM images of the as-precipitated catalyst precursor and the thermal treated catalysts. The as-precipitated molybdenum sulfide precursor is amorphous consisting of short-range disordered chains (Fig. 3a), consistent with XRD result. After thermal treatment, long-range ordered multilayer structures are formed (Fig. 3b-e). The multilayer structure reduces the exposure of rim sites, which are located on the rim of the two ends of MoS_2 along 002 direction (Fig. S3). The unpromoted catalyst (M0) possesses an interlayer distance of about

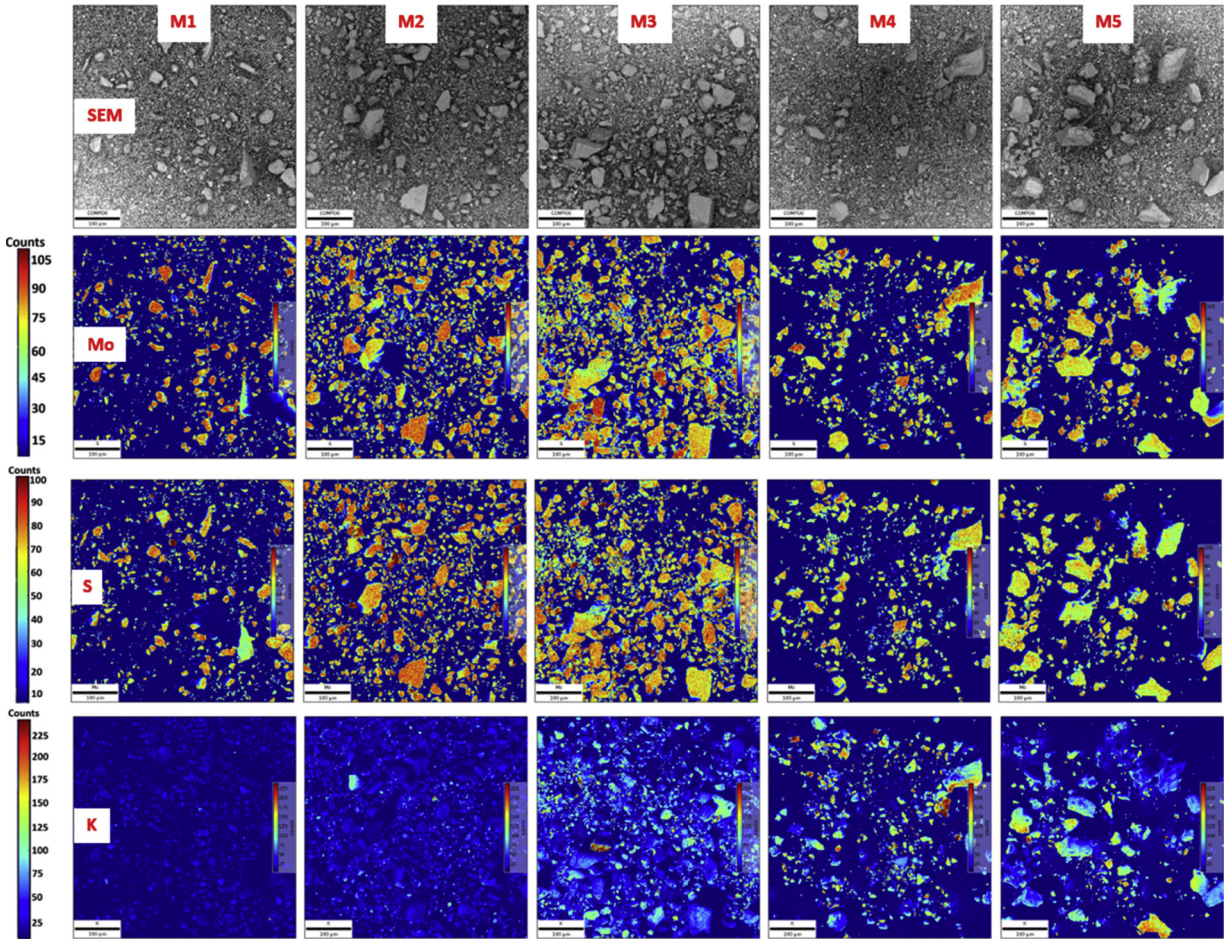

Fig. 2. SEM images and elemental mappings of molybdenum, sulfur, and potassium for potassium promoted catalysts with varying K/Mo ratio. K/Mo ratios of M1, M2, M3, M4, and M5 are 0.08, 0.15, 0.22, 0.38, and 0.52, respectively. The scale bars are 100 μm.

0.65 nm, which corresponds to the d spacing of the MoS_2 002 plane. Fig. S4 presents the interlayer distance distribution of the catalysts. With increasing K ratio, the average interlayer distance of the catalysts increases from 0.65 nm (M0) to 0.81 nm (M5), due to the insertion of potassium-containing species and formation of the $KMoS_2$ phase as indicated by the existence of the reflex at 2θ of 10° in XRD patterns [35]. Interlayer distances of about 0.64 and 0.79 nm were found between adjacent layers in M3 (Fig. 3f), confirming the existence of well-contacted MoS_2 and $KMoS_2$ phases.

Fig. 4 illustrates the Raman spectra of the catalysts. The unpromoted catalyst (M0) shows two bands at 380.8 cm^{-1} and 406.5 cm^{-1}, which are ascribed to the in-plane E^1_{2g} and out-of-plane A_{1g} vibration mode of the MoS_2 layer structure [37,38]. These two bands are also found in potassium promoted catalysts (M1, M2, M3, M4, and M5); however, the A_{1g} vibration mode shifts to lower frequency compared to M0, suggesting a bigger interlayer distance compared to M0 due to the insertion of potassium into MoS_2 interlayer space [30].

The oxidation states of potassium promoted MoS_2 depend on the precursor, the sulfurization method, and the way to incorporate potassium [39]. We studied the oxidation states of the multilayer MoS_2-$KMoS_2$ catalysts by XPS. XPS spectra of S 2p and Mo 3d are presented in Fig. S5. The doublet located at binding energies of about 161.8 eV and 163.0 eV is assigned to S $2p_{3/2}$ and S $2p_{1/2}$ of S^{2-} and/or terminal S_2^{2-}. The doublet located at about 163.4 eV and 164.6 eV is ascribed to S $2p_{3/2}$ and S $2p_{1/2}$ of bridge S_2^{2-} and/or sulfur in oxysulfide. Moreover, the peak located at 169.0 eV relates to sulfate species, which are formed due to exposure of MoS_2 to air and water [40]. The doublets at about 229.2 eV and 232.3 eV, 230.2 eV and 233.4 eV, 232.4 eV and 235.6 eV are assigned to Mo $3d_{5/2}$ and Mo $3d_{3/2}$ of Mo^{4+} (MoS_2), Mo^{5+}(MoO_xS_y), and Mo^{6+} (MoO_3), respectively [22,40,41]. Table 2 summarizes the mole percentage of Mo^{4+}, Mo^{5+}, and Mo^{6+} obtained by XPS fitting. With increasing K/Mo ratio, the percentage of the more active Mo^{4+} decreases [42], while that of Mo^{6+} increases, which is consistent with ATR-FTIR results showing MoO_3 bands at high K/Mo ratio. Under mixed alcohols synthesis conditions, only a minor portion of Mo^{6+} is reduced to Mo^{4+}, and the major portion is reduced to Mo^{5+} [43].

Summarizing the characterization results, we propose a possible formation and evolution route of potassium promoted molybdenum sulfide catalysts. The as-precipitated molybdenum sulfide precursor possesses an amorphous structure with short-range disordered molybdenum sulfide domains. Thermal treatment of the amorphous molybdenum sulfide precursor with potassium addition on one hand enables the formation of a multilayer long-range ordered structure with reduced exposure of rim sites, on the other hand it leads to the formation of well-contacted MoS_2 and $KMoS_2$ phases, respectively. While the sole MoS_2 produces mainly hydrocarbons (Scheme 1, left), the potassium promoted MoS_2 can shift the products from hydrocarbons to alcohols due to the enhanced formation of $C_xH_yO^*$ intermediates on the $KMoS_2$ phase (Scheme 1, middle). With increasing K/Mo ratio, the amount of MoS_2 phase reduces, while that of $KMoS_2$ phase increases. At the same time, the increasing K/Mo ratio leads to the formation of inactive species such as K_2SO_4, $K_2S_2O_7$, and MoO_3, which may block the active species (Scheme 1, right). With this method, a series of multilayer bifunctional MoS_2-$KMoS_2$ catalysts with reduced rim site exposure, varying composition of MoS_2/$KMoS_2$, and different active sites

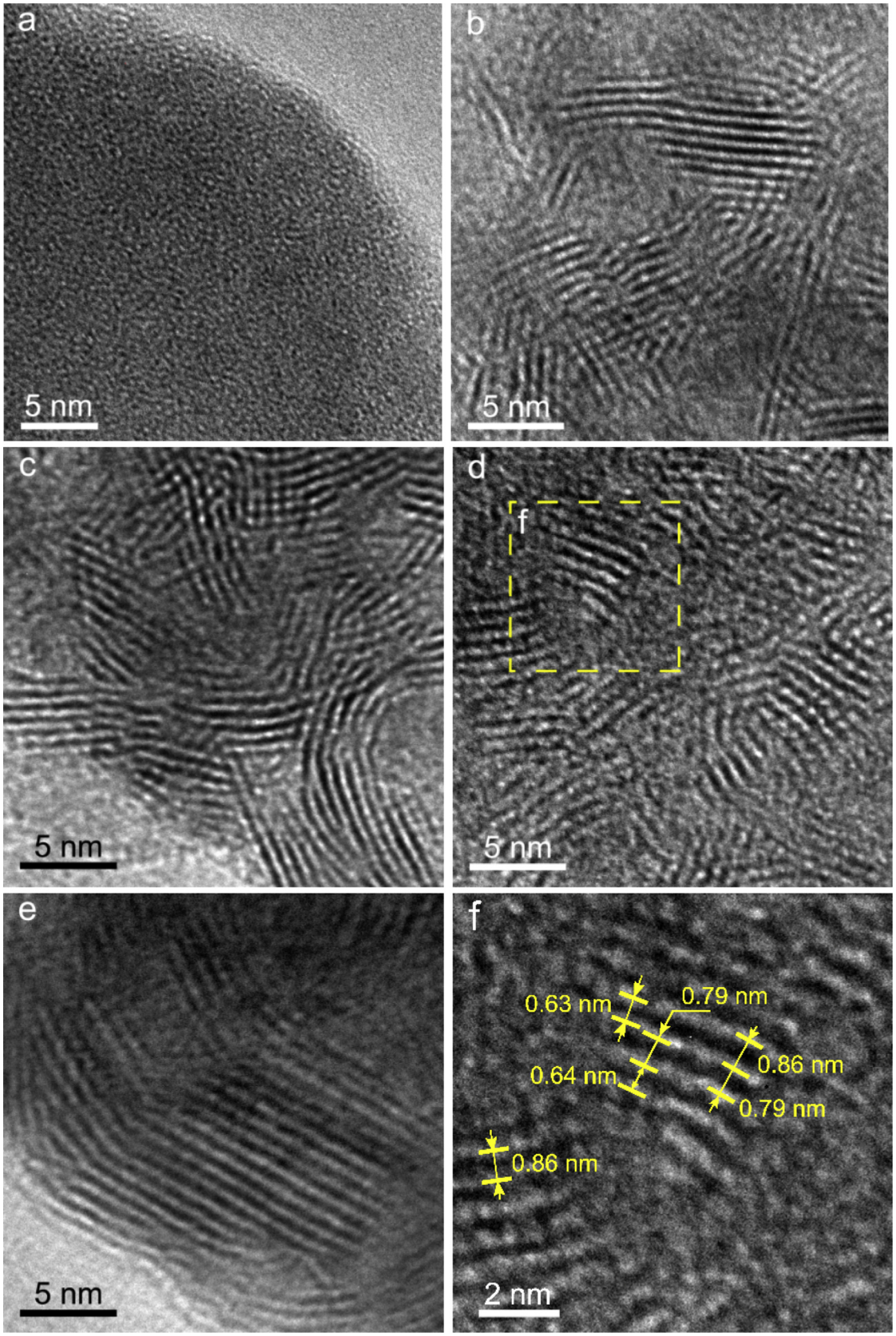

Fig. 3. TEM images of the as precipitated catalyst precursor (a) and thermal treated catalysts with varying K/Mo ratio (b–f). K/Mo ratios of M0 (b), M1 (c), M3 (d), and M5 (e) are 0, 0.08, 0.22, and 0.52, respectively. (f) is the close-view of the marked area in (d).

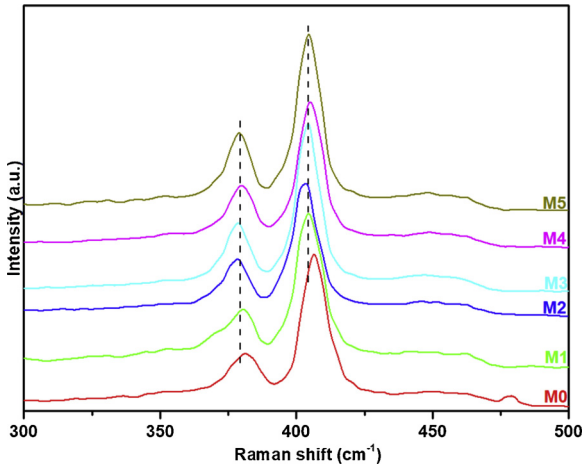

Fig. 4. Raman spectra of the catalysts with varying K/Mo ratio. K/Mo ratios of M0, M1, M2, M3, M4, and M5 are 0, 0.08, 0.15, 0.22, 0.38, and 0.52, respectively.

Table 2
Surface molybdenum oxidation states of the catalysts with varying K/Mo ratio. K/Mo ratios of M0, M1, M2, M3, M4, and M5 are 0, 0.08, 0.15, 0.22, 0.38, and 0.52, respectively.

Oxidation state	Mole percentage of Mo^{n+} (%)					
	M0	M1	M2	M3	M4	M5
Mo^{4+}	61.3	55.5	55.1	52.3	40.0	29.1
Mo^{5+}	24.4	23.1	25.7	26.7	26.0	27.5
Mo^{6+}	14.3	21.4	19.2	21.0	34.0	43.5

exposure were obtained for studying the conversion of syngas to mixed alcohols aiming for enhanced C3+ alcohols production.

3.2. Catalytic conversion of syngas to mixed alcohols

The obtained catalysts were tested in the catalytic conversion of syngas to mixed alcohols using a fixed bed reactor at 300, 340, and 380 °C, under a pressure of 8.7 MPa and a GHSV of 4500 mL g^{-1} h^{-1} with a H_2/CO ratio of 1. Fig. 5 shows the time on stream CO conversion and selectivity for M3 at 340 °C. In the first 20 h, the CO conversion and liquid oxygenates selectivity decrease, while the selectivity of hydrocarbons and CO_2 increases. Stable conversion and selectivity are obtained after 20 h, and the catalyst is stable for at least 100 h without the addition of a sulfidation agent in the feed. The 20-hour induction period, which may be due to surface sulfur loss of the catalyst and potassium-containing species redistribution during CO hydrogenation [44], is found for all the catalysts and under the different reaction conditions. However, the S/Mo ratio remains at 1.90 after 100 h catalytic test, which is almost the same as 1.89 of the fresh catalyst, indicating no significant sulfur loss and suggesting the reason for the induction period to be the redistribution of potassium containing

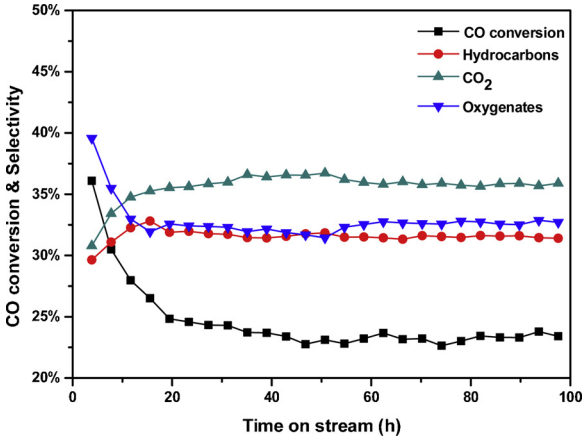

Fig. 5. Time on stream CO conversion and selectivity for M3 (K/Mo = 0.22). Reaction temperature = 340 °C, reaction pressure = 8.7 MPa, GHSV = 4500 mL g^{-1} h^{-1}, H_2/CO = 1, without sulfidation agent in the feed.

species. To obtain reliable and comparable catalytic results, we collected all the data after the induction period at a stable reaction state. The catalytic performance of the potassium promoted catalysts is summarized in Table 3. Fig. 6 presents the CO conversion of the K-MoS_2 catalysts under different reaction temperatures. The CO conversion ranges from 7.8% to 50.1%, and increases with increasing reaction temperature and decreasing K/Mo ratio. With increasing K/Mo ratio, the reduced availability of molybdenum, blockage of active sites by the inactive potassium-containing species, and the formation of inactive Mo^{6+} lead to decreased CO conversion. The unpromoted catalyst (M0) shows a low liquid oxygenate selectivity of less than 3.2% (Table S2), hindering collection of liquid product during catalytic tests for analysis and further discussion. The promoted catalysts (M1, M2, M3, M4, and M5) enable high liquid oxygenate selectivity and yields ranging from 14.2 to 46.0% and from 3.6 to 10.6%. The C3+ alcohol selectivity and yield range from 6.0 to 20.7% and from 1.6 to 5.1%, respectively.

The catalytic performance of the K-MoS_2 catalysts is further analyzed. The hydrocarbon selectivity of the catalysts under varying reaction temperature is plotted as a function of CO conversion (Fig. 7). At the same reaction temperature, the hydrocarbon selectivity decreases with increasing K/Mo ratio. As suggested by XRD, the addition of potassium leads to the formation of $KMoS_2$ and a decreased content of MoS_2. The latter is active for H_2 dissociation, while potassium promotion may decrease its hydrogenation ability. The reduced availability of active H and hydrogenation ability due to the decreasing MoS_2 content and potassium promotion are suggested to lead to a lower hydrocarbon selectivity [21,45]. For the same catalyst, hydrocarbon selectivity increases with increasing reaction temperature, because high reaction temperature favors H_2 dissociation facilitating higher hydrocarbon selectivity [46].

The CO_2 selectivity of the catalysts at varying reaction temperature is plotted as a function of CO conversion (Fig. 8). The effect of potassium and reaction temperature on the water-gas-shift reaction and CO_2 selectivity hasn't reached a consensus yet. Potassium promotion

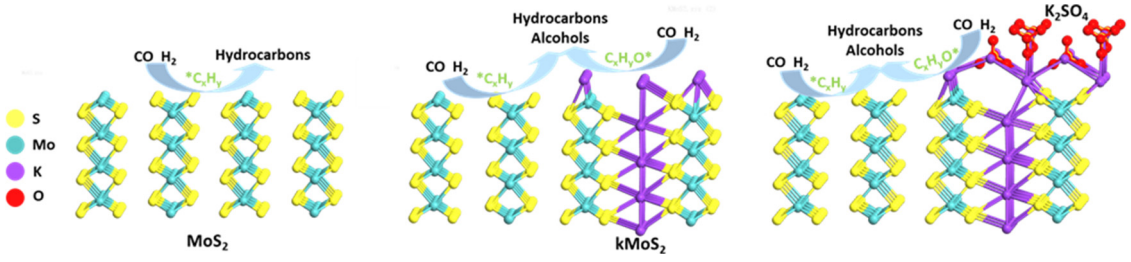

Scheme 1. The conversion of syngas to hydrocarbons and alcohols over sole MoS_2 (left), K-MoS_2 (middle), and K-MoS_2 with excessive potassium (right).

Table 3
Catalytic performance of K-MoS_2 catalysts in the conversion of syngas to mixed alcohols [a].

Catalyst[b]	T[c]/°C	X_{CO}[d]/%	Selectivity/%							Yield/%	
			CH[e]	CO_2	Oxy[f]	Methanol	Ethanol	C3 + OH[g]	Others[h]	Oxy	C3 + OH
M1	300	16.7	37.4	35.9	26.7	5.4	7.4	11.2	2.8	4.5	1.9
	340	35.2	41.6	41.0	17.4	3.1	3.9	8.5	1.9	6.1	3.0
	380	50.1	43.1	42.7	14.2	2.9	3.8	6.0	1.5	7.1	3.0
M2	300	11.8	29.8	31.2	39.0	6.3	11.5	17.6	3.6	4.6	2.1
	340	30.4	36.8	39.0	24.2	3.9	6.7	11.1	2.4	7.4	3.4
	380	42.6	38.7	41.6	19.7	4.1	6.8	8.4	0.5	8.4	3.6
M3	300	9.6	23.7	30.8	45.5	7.6	15.0	20.7	2.2	4.4	2.0
	340	24.3	31.5	35.8	32.7	4.7	10.2	14.9	2.9	7.9	3.6
	380	39.1	33.6	40.0	26.4	4.6	9.0	11.3	1.4	10.3	4.4
M4	300	8.2	23.5	32.5	44.0	7.8	15.4	19.0	1.7	3.6	1.6
	340	22.1	30.8	37.4	31.8	5.6	11.1	13.3	1.8	7.0	2.9
	380	38.4	32.6	40.3	27.1	5.1	9.1	11.2	1.7	10.4	4.3
M5	300	7.8	22.9	31.1	46.0	6.7	13.7	20.6	5.0	3.6	1.6
	340	20.8	30.0	36.5	33.5	5.1	10.7	15.3	2.4	7.0	3.2
	380	36.5	31.2	39.7	29.1	3.9	8.0	14.0	3.2	10.6	5.1

[a] Reaction pressure = 8.7 MPa, GHSV = 4500 mL g^{-1} h^{-1}, H_2/CO = 1.
[b] K/Mo ratios of M1, M2, M3, M4, and M5 are 0.08, 0.15, 0.22, 0.38, and 0.52, respectively.
[c] Reaction temperature.
[d] CO conversion.
[e] Hydrocarbons.
[f] Liquid oxygenate.
[g] C3+ alcohols.
[h] Other liquid oxygenate except alcohols.

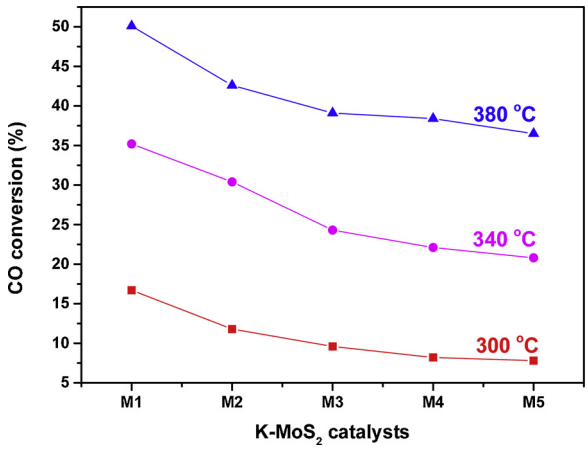

Fig. 6. The CO conversion over K-MoS_2 catalysts at reaction temperatures of 300, 340, and 380 °C. K/Mo ratios of M1, M2, M3, M4, and M5 are 0.08, 0.15, 0.22, 0.38, and 0.52, respectively. Reaction pressure = 8.7 MPa, GHSV = 4500 mL g^{-1} h^{-1}, H_2/CO = 1.

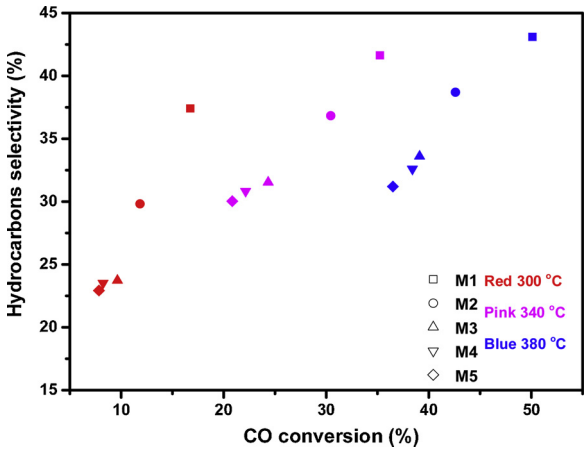

Fig. 7. Hydrocarbons selectivity as a function of CO conversion. K/Mo ratios of M1, M2, M3, M4, and M5 are 0.08, 0.15, 0.22, 0.38, and 0.52, respectively. Reaction pressure = 8.7 MPa, GHSV = 4500 mL g^{-1} h^{-1}, H_2/CO = 1.

was described to either enhance or weaken the water-gas-shift reaction depending on the catalyst synthesis procedure [19,21,47,48]. The water-gas-shift reaction is favored at low reaction temperature, because the equilibrium constant of the equilibrium-controlled water-gas-shift reaction decreases with increasing temperature; however, higher reaction temperatures are usually required to achieve a sufficient reaction rate [49]. Thus, inversed influences of temperature on water-gas-shift reaction are reported. Lower equilibrium CO content is found at lower reaction temperature for the water-gas-shift reaction, while an increased CO_2 selectivity with raising reaction temperature is found for mixed alcohols synthesis [47,49]. In this work, a high K/Mo ratio leads to low CO_2 selectivity, and CO_2 selectivity increases with increasing reaction temperature. A nearly linear relation of CO_2 selectivity and CO conversion occurs. The formation of alcohols and hydrocarbons consumes H_2 and CO with a ratio of higher than 2, indicating H_2 is consumed faster with increasing CO conversion. Also H_2O is formed as a side product of these two reactions. With increasing CO conversion, the consumption of H_2 and the formation of H_2O drive the water-gas-shift reaction to the formation of CO_2 and H_2.

The liquid oxygenate selectivity of the catalysts under varying reaction temperature is plotted as a function of CO conversion (Fig. 9). The liquid oxygenate selectivity decreases with increasing reaction temperature, and increases with increasing K/Mo ratio. The liquid oxygenate selectivity changes only slightly from M3 to M5. A possible reason is the blockage of $KMoS_2$ site by the inactive K_2SO_4 and $K_2S_2O_7$ species, respectively. The high liquid oxygenate selectivity at high K/Mo ratio and low reaction temperature benefits from the inhibited formation of hydrocarbons and CO_2, and enhanced formation of alcohols. With raising K/Mo ratio, the increasing content of $KMoS_2$ appears to favors a non-dissociative CO adsorption enhancing alcohols formation [45]. The highest liquid oxygenate selectivity of about 45% is obtained by M3, M4, and M5 at a reaction temperature of 300 °C. However, the liquid oxygenate yield is too low under such conditions due to the low CO conversion. Fig. 10 presents the relationship between liquid oxygenate yield and selectivity. Relatively high yield and

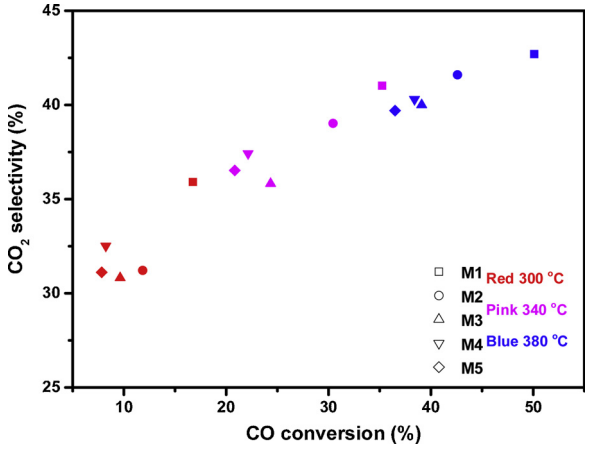

Fig. 8. CO_2 selectivity as a function of CO conversion. K/Mo ratios of M1, M2, M3, M4, and M5 are 0.08, 0.15, 0.22, 0.38, and 0.52, respectively. Reaction pressure = 8.7 MPa, GHSV = 4500 mL $g^{-1} h^{-1}$, H_2/CO = 1.

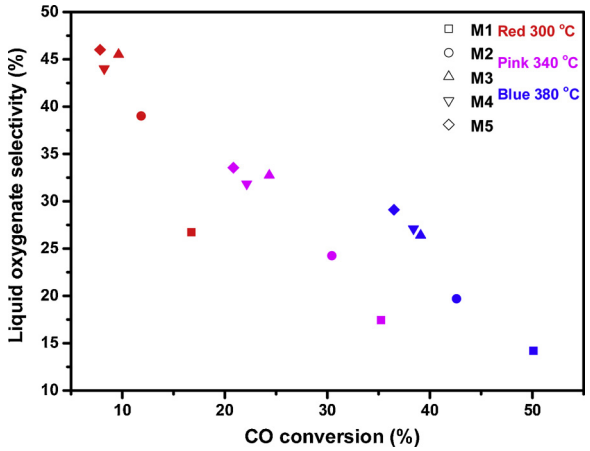

Fig. 9. Liquid oxygenate selectivity as a function of CO conversion. K/Mo ratios of M1, M2, M3, M4, and M5 are 0.08, 0.15, 0.22, 0.38, and 0.52, respectively. Reaction pressure = 8.7 MPa, GHSV = 4500 mL $g^{-1} h^{-1}$, H_2/CO = 1.

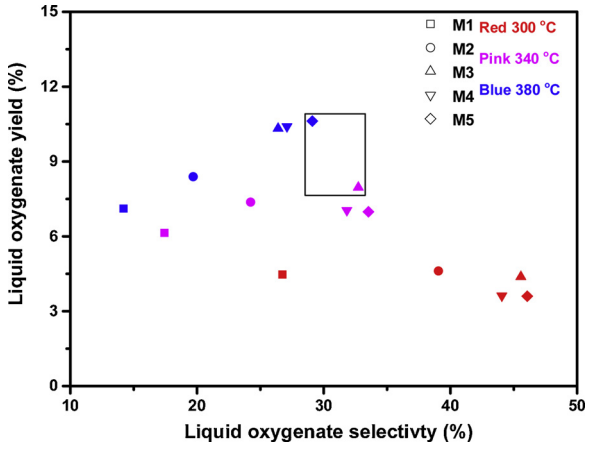

Fig. 10. Liquid oxygenate yield as a function of liquid oxygenate selectivity. K/Mo ratios of M1, M2, M3, M4, and M5 are 0.08, 0.15, 0.22, 0.38, and 0.52, respectively. Reaction pressure = 8.7 MPa, GHSV = 4500 mL $g^{-1} h^{-1}$, H_2/CO = 1.

selectivity are obtained by M3 at 340 °C and M5 at 380 °C located in the rectangle in Fig.10. M3 and M5 provide liquid oxygenate yields of 7.9 and 10.6% as well as a selectivity of 32.7 and 29.1%, respectively.

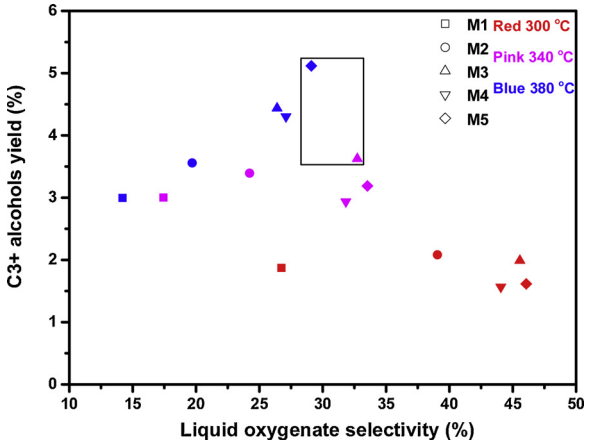

Fig. 11. C3+ alcohol yield as a function of liquid oxygenate selectivity. K/Mo ratios of M1, M2, M3, M4, and M5 are 0.08, 0.15, 0.22, 0.38, and 0.52, respectively. Reaction pressure = 8.7 MPa, GHSV = 4500 mL $g^{-1} h^{-1}$, H_2/CO = 1.

Fig. 11 shows the relationship between C3+ alcohol yield and liquid oxygenate selectivity. M3 at 340 °C and M5 at 380 °C also enable a relatively high C3+ alcohol yield and liquid oxygenate selectivity reaching a C3+ alcohol yield of 3.6 and 5.1%, respectively. C3+ alcohols account for more than 46% (carbon atom fraction) of the liquid oxygenate. The optimized liquid oxygenate selectivity and yield are in line with the literature benchmarks of molybdenum based catalysts (Table S3).

The alcohol distribution and chain growth are further studied. ASF distribution, $S_n/n = \alpha^{n-1}(1-\alpha)$, is used to illustrate the alcohols distribution and calculate the chain growth probability. S_n% is the carbon selectivity of alcohols with a carbon number of n, n is the carbon number, and α is the chain growth probability. A linear relationship is expected between $\ln(S_n/n)$ and $(n-1)$. Fig. 12 shows the alcohol distribution over M3 at 340 °C (the distributions over other catalysts are presented in Fig. S6). $\ln(S_n/n)$ of C3+ alcohols shows a linear relation versus $(n-1)$ following ASF distribution, while a deviation of methanol and ethanol from the ASF distribution occurs. The loss of methanol and ethanol due to incomplete condensation was estimated. Less than 1% increase of methanol selectivity and no significant increase of ethanol selectivity were found, indicating the deviation is not due to the loss of methanol and ethanol. With increasing K/Mo ratio, the deviation of methanol and ethanol from ASF distribution increases from M0 to M3

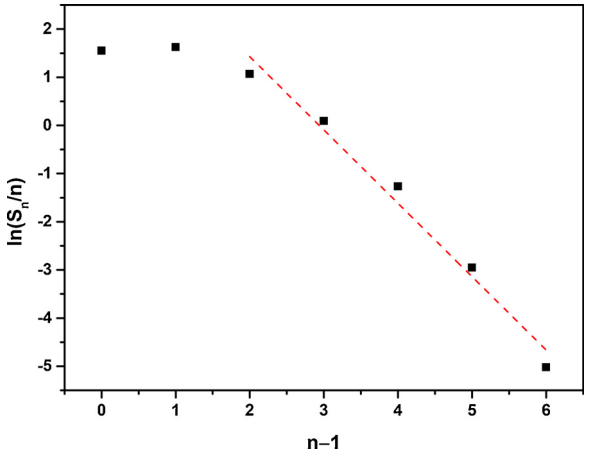

Fig. 12. ASF distributions of alcohols over M3 (K/Mo = 0.22). Reaction temperature = 340 °C, reaction pressure = 8.7 MPa, GHSV = 4500 mL $g^{-1} h^{-1}$, H_2/CO = 1. The points are measure data, and the dash lines are ASF fittings for C3+ alcohols.

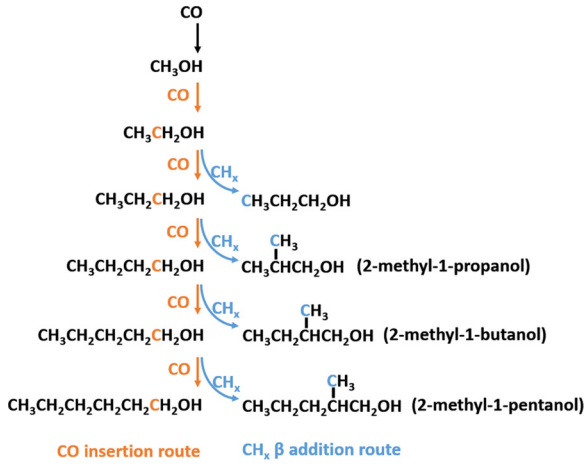

Scheme 2. The formation of the alcohols through CO insertion and CH_x β-addition. The orange carbon atoms are added though CO insertion and the blue carbon atoms are added via CH_x β-addition.

and fluctuates slightly from M3 to M5 as indicated by the angel between the fitting line of methanol and ethanol, and C3+ alcohols (Fig. S6). The deviation implies a different chain growth mechanism of C3+ alcohols compared to that of ethanol [24,50,51]. The two possible chain growth mechanisms are CO insertion and CH_x addition. The chain growth probabilities calculated with C3+ alcohols range from 0.2 to 0.3 (Table S4).

To further study the chain growth mechanism, the composition of the produced alcohols is analyzed. Fig. S7 summarizes the mole ratio of isomeric alcohols to the respective linear primary alcohols over different catalysts, and Scheme 2 presents the formation of the main products through CO insertion and CH_x β-addition. The main isomeric alcohols are 2-methyl-1-propanol, 2-methyl-1-butanol, and 2-methyl-1-pentanol. As shown in Scheme 2, the linear primary alcohols are formed through CO insertion, while the branched alcohols, 2-methy-1-propanol, 2-methyl-1-butanol, and 2-methyl-1-pentanol, are formed by joint CO insertion and CH_x β-addition, which is responsible for the growth of the branched chain [24]. Propanol may be formed through both routes. The two chain growth mechanisms, CO insertion for ethanol, and joint CO insertion and CH_x β-addition for C3+ alcohols are consistent with the deviation from ASF distribution. At a low K/Mo ratio, M1 shows a low branched alcohols/linear primary alcohols ratio of less than 0.4. With increasing K/Mo ratio, the branched alcohols/linear primary alcohols ratios increase and reach a maximum of about 0.9 with M3. The branched alcohols/linear primary alcohols ratios decrease slightly with further increasing K/Mo ratio (M4 and M5). Since CH_x is formed on MoS_2 [52], and CO adsorption happens on $KMoS_2$, a good contact and balance between these two phases are of great importance for the chain growth through CH_x β-addition and CO insertion. The multilayer structure of the catalyst with potassium located in the interlayer space enables good contact between the two phases. With low K/Mo ratio, the CH_x tends to form CH_4, however the availability of CH_x decreases with increasing K/Mo. Thus, the formation of branched alcohols reaches a maximum with medium potassium promotion, too high or too low K/Mo ratio weakens the branched alcohols formation. By tailoring the K/Mo ratio, the chain growth through CO insertion and CH_x β-addition is optimized enabling an enhanced C3+ alcohol production with high liquid oxygenate yield and selectivity.

4. Conclusion

We report a method for tailoring the structure of potassium promoted MoS_2 catalysts to produce mixed alcohols with enhanced C3+ alcohol production. The preparation of potassium promoted MoS_2 by thermal treatment of a mixture of amorphous $MoS_{3.7}$ and K_2CO_3 leads to the formation of a multilayer structure with MoS_2 and K-MoS_2 mixed phases. The multilayer structure with reduced exposure of rim sites and well-contacted MoS_2 and $KMoS_2$ phase fosters carbon chain growth and C3+ alcohol production, and allows deviating from the ASF distribution of the alcohols through enhanced CO insertion and CH_x β-addition. By tailoring the K/Mo ratio, catalysts with different relative ratio of $KMoS_2$ and MoS_2 phases were obtained to optimize the formation of liquid oxygenates with enhance C3+ alcohol production under appropriate reaction temperature. High liquid oxygenate selectivity and yield of 29.1–32.7% and 7.9–10.6%, and high C3+ alcohols content in the liquid oxygenates and a high C3+ alcohol yield of 46% and 3.6–5.1%, respectively, as well as good stability are obtained by catalyst design and optimizing the reaction condition.

Conflicts of interest

The authors declare that they have no conflicts of interest.

Acknowledgements

Feng Zeng and Xiaoying Xi acknowledge China Scholarship Council (CSC) for financial support. Regina Palkovits acknowledges the project house P2F (Competence Center Power to Fuel) of RWTH Aachen University financed by the Excellence Initiative of the German federal and state governments to promote science and research at German universities.

References

[1] S. Yeh, Energy Policy 35 (2007) 5865–5875.
[2] G.A. Olah, Angew. Chem. Int. Ed. 44 (2005) 2636–2639.
[3] L.P. Wackett, Curr. Opin. Chem. Biol. 12 (2008) 187–193.
[4] J. Hill, E. Nelson, D. Tilman, S. Polasky, D. Tiffany, Proc. Natl. Acad. Sci. 103 (2006) 11206–11210.
[5] H. Balat, E. Kırtay, Int. J. Hydrogen Energy 35 (2010) 7416–7426.
[6] G.-H. Tzeng, C.-W. Lin, S. Opricovic, Energy Policy 33 (2005) 1373–1383.
[7] W.-D. Hsieh, R.-H. Chen, T.-L. Wu, T.-H. Lin, Atmos. Environ. 36 (2002) 403–410.
[8] S. Liu, E.R.C. Clemente, T. Hu, Y. Wei, Appl. Therm. Eng. 27 (2007) 1904–1910.
[9] J. Vancoillie, J. Demuynck, L. Sileghem, M. Van De Ginste, S. Verhelst, Int. J. Hydrogen Energy 37 (2012) 9914–9924.
[10] E. Christensen, J. Yanowitz, M. Ratcliff, R.L. McCormick, Energy Fuels 25 (2011) 4723–4733.
[11] N.S. Shamsul, S.K. Kamarudin, N.A. Rahman, N.T. Kofli, Renew. Sustain. Energy Rev. 33 (2014) 578–588.
[12] F.W. Bai, W.A. Anderson, M. Moo-Young, Biotechnol. Adv. 26 (2008) 89–105.
[13] H.T. Luk, C. Mondelli, D.C. Ferré, J.A. Stewart, J. Pérez-Ramírez, Chem. Soc. Rev. 46 (2017) 1358–1426.
[14] D. Sutton, B. Kelleher, J.R. Ross, Fuel Process. Technol. 73 (2001) 155–173.
[15] D. Pakhare, J. Spivey, Chem. Soc. Rev. 43 (2014) 7813–7837.
[16] T.L. LeValley, A.R. Richard, M. Fan, Int. J. Hydrogen Energy 39 (2014) 16983–17000.
[17] M. Ni, J. Power Sour. 202 (2012) 209–216.
[18] K. Fang, D. Li, M. Lin, M. Xiang, W. Wei, Y. Sun, Catal. Today 147 (2009) 133–138.
[19] V.R. Surisetty, A. Tavasoli, A.K. Dalai, Appl. Catal. Gen. 365 (2009) 243–251.
[20] H. Qi, D. Li, C. Yang, Y. Ma, W. Li, Y. Sun, B. Zhong, Catal. Commun. 4 (2003) 339–342.
[21] X. Li, L. Feng, Z. Liu, B. Zhong, D.B. Dadyburjor, E.L. Kugler, Ind. Eng. Chem. Res. 37 (1998) 3853–3863.
[22] C. Liu, M. Virginie, A. Griboval-Constant, A.Y. Khodakov, Catal. Today 261 (2016) 137–145.
[23] X. Kang, B.A.O. Zhenghong, Q.I. Xingzhen, W. Xinxing, L. ZHONG, F. Kegong, L.I.N. Minggui, S.U.N. Yuhan, Chin. J. Catal. 34 (2013) 116–129.
[24] D. Li, C. Yang, W. Li, Y. Sun, B. Zhong, Top. Catal. 32 (2005) 233–239.
[25] P.L. Spath, D.C. Dayton, Preliminary Screening–Technical and Economic Assessment of Synthesis Gas to Fuels and Chemicals With Emphasis on the Potential for Biomass-derived Syngas, National Renewable Energy Lab., Golden, CO.(US), 2003.
[26] V.R. Surisetty, A.K. Dalai, J. Kozinski, Appl. Catal. Gen. 385 (2010) 153–162.
[27] D. Li, N. Zhao, H. Qi, W. Li, Y.H. Sun, B. Zhong, Catal. Commun. 6 (2005) 674–678.
[28] D. Li, C. Yang, H. Qi, H. Zhang, W. Li, Y. Sun, B. Zhong, Catal. Commun. 5 (2004) 605–609.
[29] V.S. Dorokhov, D.I. Ishutenko, P.A. Nikul'shin, K.V. Kotsareva, E.A. Trusova, T.N. Bondarenko, O.L. Eliseev, A.L. Lapidus, N.N. Rozhdestvenskaya, V.M. Kogan, Kinet. Catal. 54 (2013) 243–252.
[30] M.T. Claure, S.-H. Chai, S. Dai, K.A. Unocic, F.M. Alamgir, P.K. Agrawal,

C.W. Jones, J. Catal. 324 (2015) 88–97.
[31] F. Zeng, C. Broicher, S. Palkovits, K. Simeonov, R. Palkovits, Catal. Sci. Technol. 8 (2018) 367–375.
[32] W. Mao, J. Su, Z. Zhang, X.-C. Xu, D. Fu, W. Dai, J. Xu, X. Zhou, Y.-F. Han, Chem. Eng. Sci. 135 (2015) 301–311.
[33] P.B. Weisz, C.D. Prater, Adv. Catal. Elsevier, 1954, pp. 143–196.
[34] M.-R. Gao, M.K. Chan, Y. Sun, Nat. Commun. 6 (2015) 7493.
[35] L. Chen, F. Chen, N. Tronganh, M. Lu, Y. Jiang, Y. Gao, Z. Jiao, L. Cheng, B. Zhao, J. Mater. Res. 31 (2016) 3151–3160.
[36] R. Zhang, I.-L. Tsai, J. Chapman, E. Khestanova, J. Waters, I.V. Grigorieva, Nano Lett. 16 (2015) 629–636.
[37] H. Li, Q. Zhang, C.C.R. Yap, B.K. Tay, T.H.T. Edwin, A. Olivier, D. Baillargeat, Adv. Funct. Mater. 22 (2012) 1385–1390.
[38] M. Thripuranthaka, R.V. Kashid, C. Sekhar Rout, D.J. Late, Appl. Phys. Lett. 104 (2014) 081911.
[39] A. Cordova, P. Blanchard, C. Lancelot, G. Frémy, C. Lamonier, ACS Catal. 5 (2015) 2966–2981.
[40] L. Qiu, G. Xu, Appl. Surf. Sci. 256 (2010) 3413–3417.
[41] L. Benoist, D. Gonbeau, G. Pfister-Guillouzo, E. Schmidt, G. Meunier, A. Levasseur, Thin Solid Films 258 (1995) 110–114.
[42] M. Saito, R.B. Anderson, J. Catal. 63 (1980) 438–446.
[43] X.-M. Wu, Y.-Y. Guo, J.-M. Zhou, G.-D. Lin, X. Dong, H.-B. Zhang, Appl. Catal. Gen. 340 (2008) 87–97.
[44] H. Xiao, D. Li, W. Li, Y. Sun, Fuel Process. Technol. 91 (2010) 383–387.
[45] V.P. Santos, B. van der Linden, A. Chojecki, G. Budroni, S. Corthals, H. Shibata, G.R. Meima, F. Kapteijn, M. Makkee, J. Gascon, ACS Catal. 3 (2013) 1634–1637.
[46] L. Jalowiecki, J. Grimblot, J.P. Bonnelle, J. Catal. 126 (1990) 101–108.
[47] T. Tatsumi, A. Muramatsu, H. Tominaga, J. Jpn. Pet. Inst. 35 (1992) 233–243.
[48] R.N. Nickolov, R.M. Edreva-Kardjieva, V.J. Kafedjiysky, D.A. Nikolova, N.B. Stankova, D.R. Mehandjiev, Appl. Catal. Gen. 190 (2000) 191–196.
[49] D.S. Newsome, Catal. Rev. Sci. Eng. 21 (1980) 275–318.
[50] R.W. Dorner, D.R. Hardy, F.W. Williams, B.H. Davis, H.D. Willauer, Energy Fuels 23 (2009) 4190–4195.
[51] J. Patzlaff, Y. Liu, C. Graffmann, J. Gaube, Appl. Catal. Gen. 186 (1999) 109–119.
[52] A.B. Anderson, J.J. Maloney, J. Yu, J. Catal. 112 (1988) 392–400.